Improved method of estimating temperatures at meteor peak heights

Emranul Sarkar[1,2], Alexander Kozlovsky[1], Thomas Ulich[1], Ilkka Virtanen[2], Mark Lester[3], and Bernd Kaifler[4]

[1]Sodankylä Geophysical Observatory, Sodankylä, Finland
[2]Space Physics and Astronomy Research Unit, University of Oulu, Finland
[3]Department of Physics and Astronomy, University of Leicester, Leicester, UK
[4]Deutsches Zentrum für Luft- und Raumfahrt, Institut für Physik der Atmosphäre, Oberpfaffenhofen, Germany

Correspondence: Emranul Sarkar (emranul.sarkar@oulu.fi)

Abstract.

For two decades meteor radars have been routinely used to monitor atmospheric temperature around 90 km altitude. A common method, based on a temperature-gradient model, is to use the height dependence of meteor decay time to obtain a height-averaged temperature in the peak meteor region. Traditionally this is done by fitting a linear regression model in the scattered plot of $log_{10}(1/\tau)$ and height, where τ is the half-amplitude decay time of the received signal. However, this method was found to be consistently biasing the slope estimate. The consequence of such bias is that it produces a systematic offset in the estimated temperature, and thus requiring calibration with other colocated measurements. The main reason for such a biasing effect is thought to be due to the failure of the classical regression model to take into account the measurement error in τ and the observed height. This is further complicated by the presence of various geophysical effects in the data, as well as observational limitation in the measuring instruments. To incorporate various error terms in the statistical model, an appropriate regression analysis for these data is the Errors-in-Variables model. An initial estimate of the slope parameter is obtained by assuming symmetric error variances in normalised height and $log_{10}(1/\tau)$. This solution is found to be a good prior estimate for the core of this bivariate distribution. Further improvement is achieved by defining density contours of this bivariate distribution and restricting the data selection process within higher contour levels. With this solution, meteor radar temperatures can be obtained independently without needing any external calibration procedure. When compared with colocated lidar measurements, the systematic offset in the estimated temperature is shown to have reduced to 5% or better on average.
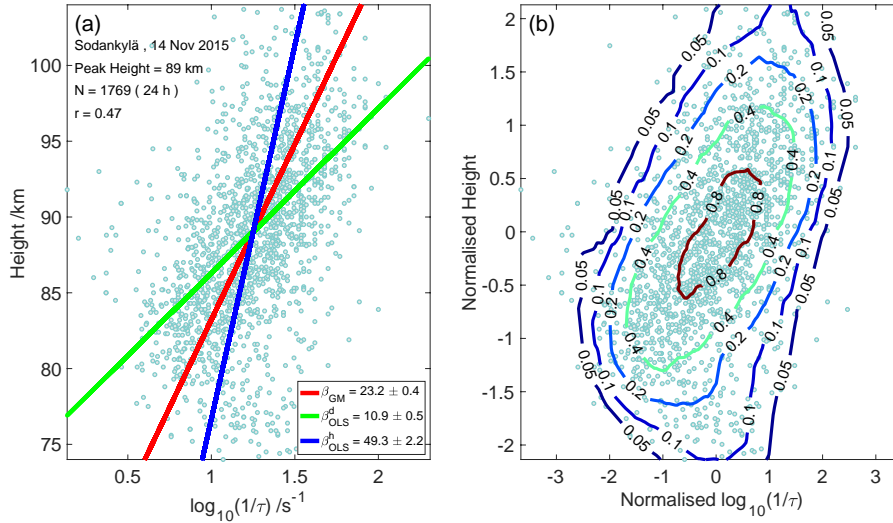
Figure 1. (a) Typical scatter plot of $log_{10}(1/\tau)$ and height. The lines correspond to best fit models using different regression methods described in the text. The *green* and *blue* line corresponds to 'ordinary least-squares method (OLS)' with $log_{10}(1/\tau)$ and height as independent variable respectively. The *red* line correspond to the geometric mean (GM) of β_{OLS}^{d} and β_{OLS}^{h}. (b) The bivariate distribution of the data. The measured height and $log_{10}(1/\tau)$ are converted to dimension free coordinates using Eq. (18). The relative density contours are obtained by counting the number of detections in a circle of unit area relative to the detection density at the height of peak meteor occurrences at the center.

1 Introduction and background

20 As meteoroids enter the Earth's atmosphere, they produce ionized trails which can be detected as back-scattered radio signals by interferometric radars. After the trail has been formed, the ionisation begins to dissipate by various processes, such as, ambipolar diffusion, eddy diffusion, or electron loss due to recombination and attachment depending on the height of ablation. The rate at which the echo power decreases is also determined by the combined effect of electron line density of the trail, ambient pressure and temperature.

25 If the electron line density of the trail is less than 2.4×10^{14} electrons m^{-1}, the trail is called 'underdense', meaning each electron in the trail scatters independently (e.g., Bronshten, 1983, p 356). The decay of underdense trails is thought to be mainly due to ambipolar diffusion at a height range of 85–95 km, where the majority of the meteors ablate (Jones, 1975). In the weak scattering limit the backscattered amplitude of the radio signal from an underdense trail decays with time (t) as

$$A(t) = A(0)e^{-16\pi^2 D_a t/\lambda_r^2} \tag{1}$$

30 where λ_r is the radar wavelength and D_a is the ambipolar diffusion coefficient (Kaiser, 1953). This coefficient depends on the ambient pressure (P) and temperature (T) of the neutral gas (Chilson et al., 1996) and can be estimated from the half-amplitude

decay time (τ) as

$$D_a = K_{amb}\frac{T^2}{P} = \frac{\lambda_r^2\, ln2}{16\pi^2\tau} \tag{2}$$

K_{amb} in Eq. (2) is a constant related to the ionic constituent of the plasma in the trail (Hocking et al., 1997). The pressure at a given height (h) is

$$P(h) = P(0)e^{-\int_0^h \frac{mg}{kT(z)}dz} \tag{3}$$

where m is the mass of a typical atmospheric molecule, g is the acceleration of gravity, k is the Boltzmann constant, z is an axis along the vertical. Substituting the equation for pressure in Eq. (2), and differentiating provides the height profile of the decay time:

$$log_{10}D_a(h) = 2log_{10}T(h) + log_{10}e\frac{mg}{k}\int_0^h \frac{1}{T(z)}dz + \Psi \tag{4}$$

$$\frac{d}{dh}log_{10}(\frac{1}{\tau(h)}) = 2\,log_{10}e\,\frac{dT}{dh}\frac{1}{T(h)} + log_{10}e\,\frac{mg}{k}\frac{1}{T(h)} \tag{5}$$

where Ψ is a constant. Equation (5) states that the height profile of decay time is a function of both temperature and temperature gradient under the assumption of ambipolar diffusion for underdense meteor trails. In practice, most trail echoes are received at a small altitude range referred to as the region of peak meteor occurrence (Hocking, 1999). Hence a height-averaged temperature gradient near the peak height can be used to estimate the mean temperature (T_0) at the peak height by fitting a linear function (Hocking, 1999). A linear approximation of Eq. (5) is,

$$T_0 = \beta\,(2 < \frac{dT}{dh} > + \frac{mg}{k})\,log_{10}e \tag{6}$$

where β is the slope of the scattered plot of $log_{10}(1/\tau)$ and height, and T_0 is the average temperature of the atmosphere at the height of peak meteor occurrence. A typical scattered plot of height and $log_{10}(1/\tau)$ shows significant variation in the measured data along both abscissa and ordinate (Fig. 1). Traditionally, the slope (β) is estimated using the ordinary least-squares (OLS) method with $log_{10}(1/\tau)$ as the independent variable. The justification of using $log_{10}(1/\tau)$ as independent variable is that the measurement errors in τ are smaller than those in heights (Hocking et al., 1997). While the pulse length, angular resolution etc., of the radar introduces intrinsic measurement errors in heights, much of the variation in decay time is due to various geophysical effects that persist at all altitudes. At higher altitude the collision frequency with neutrals is reduced, and the diffusion is inhibited in a direction orthogonal to the geomagnetic field (Jones, 1991; Robson, 2001). This anisotropic diffusion causes an increase in the duration of meteor radar echoes as compared to ambipolar diffusion. Whereas at lower altitude decay time tends to decrease due to additional effect of electron loss by recombination and attachment (Younger et al., 2008). In addition, other geophysical factors, such as meteor fragmentation, turbulence within trail, chemical composition of the meteors, or the temperature variation due to passage of tides and gravity waves, can contribute to the measurements of decay time and heights at all altitudes (Hocking, 2004).

Temperature estimation from meteor radar (MR) data requires obtaining the best-fit regression line in the scattered plot of $log_{10}(1/\tau)$ and height. However, the pioneer work done by Hocking (1999) to implement this method using ordinary least-squares fitting showed a clear systematic offset between the MR temperature and colocated lidar measurements, indicating that the estimated slope was not determined correctly. To correct for this offset, a common practice is to calibrate the meteor radar temperatures using temperatures from lidar, OH spectrometer, satellite or rocket climatology. Hocking et al. (2001b) provided a *statistical comparison technique (SCT)* to calibrate the biased slope estimate as,

$$\beta^d_{OLS} = (1 - \frac{s_\delta}{s_d}) \beta_{SCT} \tag{7}$$

Or,

$$\beta_{SCT} = (1 - \frac{s_\varepsilon}{s_h}) \beta^h_{OLS} \tag{8}$$

where s_δ and s_ε are the error variances of the (log of) diffusion coefficient (or decay time) and height respectively, s_d and s_h are data variances of $log_{10}(1/\tau)$ and of height respectively, β^d_{OLS} and β^h_{OLS} are slope coefficients when diffusion coefficient or height is treated as independent variable respectively in the OLS regression analysis. The calibrated slope, β_{SCT}, is traditionally obtained by arbitrarily choosing s_δ or s_ε that gives the best temperature estimates of MR as compared to optical or satellite data (e.g., Holdsworth et al., 2006; Hocking et al., 2007; Kim et al., 2012). A severe shortcoming of such calibration procedure is that the calibration factors (s_δ and s_ε) in the parenthesis of Eq. (7) or Eq. (8) are dependent on the data selection criteria (e.g., limiting heights, decay time or zenith angle to a certain range). Moreover, the outcome of any such calibration routine will depend on the location of the MR and the choice of the calibration instrument. From a pure statistical context, the arbitrary choice of calibration parameters makes the estimated temperature also an arbitrary quantity thereby making it impossible to draw any reasonable statistical inferences.

In practice, the ordinary least-squares method will not be valid for MR data since neither the height nor the decay time can be predetermined as independent variable, and both variables are subjected to intrinsic measurement errors and various geophysical effects. The reasons for such bias, and thus needing calibration, is discussed on theoretical and experimental grounds in Sect. 3.1. In addition, a statistical procedure to estimate s_δ and s_ε using SCT calibration is formulated and presented in Sect. 3.1. An alternative method that includes measurement errors in the regression model is introduced in Sect. 3.2. This analysis does not require an absolute knowledge of s_δ or s_ε, but only the relative value is needed. As an alternative to SCT calibration, in Sect. 4, an independent slope estimation is obtained using the Errors-in-Variables model. A comparison study of the estimated MR temperatures with colocated lidar temperatures is discussed to validate the method.

2 Instrumentation and data

The All-Sky Interferometric Meteor Radar (SKiYMET) at Sodankylä Geophysical Observatory (SGO, 67°22' N, 26°38' E, Finland) has been routinely monitoring daily meteor-height averaged temperatures and wind velocity since December 2008 (Kozlovsky et al., 2016). The radar operates at a transmission power of 15 kW and frequency of 36.9 MHz, with a transmitting
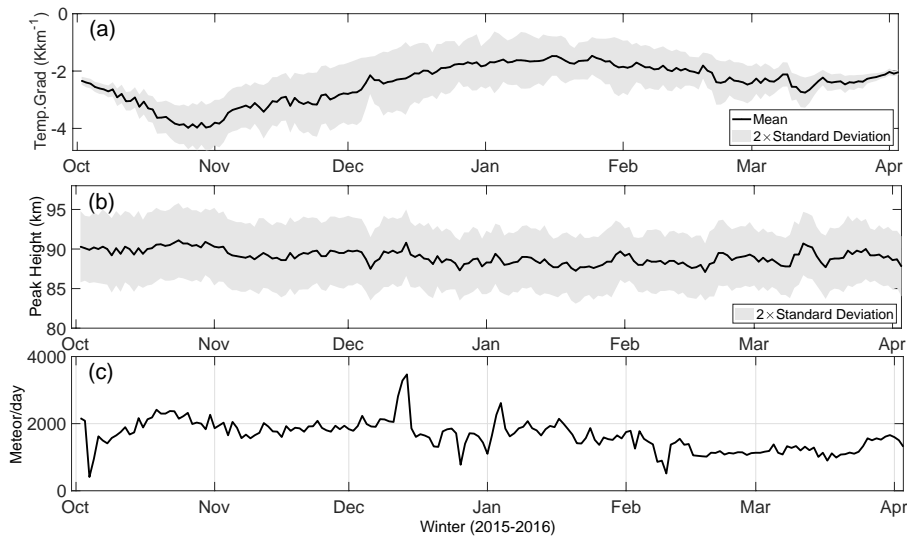
Figure 2. (a) Temperature gradient model derived from MSIS90. (b) Peak meteor heights for the data used in this work, and (c) the daily meteor detection for zenith angle less than $50°$ and velocity in the range ±100 m/s.

antenna which has a broad radiation pattern designed to illuminate a large expanse of the sky. The meteor trails are detected within a circle of 300 km diameter around SGO. The phase differences in the five-antennae receiving array allow the determi-
95 nation of the azimuth, elevation, range, and line-of-sight Doppler velocity of the meteor trails. The 2144 Hz pulse repetition frequency of MR transmission introduces a range ambiguity of 70 km, and the built-in analysis software therefore assumes meteor trails are within the height of 70 to 110 km for unambiguous detections. Uncertainty in the height is ±1 km (or better for large zenith angle), which is determined by the 2 km range resolution. In addition, the half-time (τ) of the received signal is calculated from the width of the autocorrelation function. A detailed description of the algorithm of the SKiYMET signal
100 processing software is outlined in Hocking et al. (2001a).

SGO is located at the corrected geomagnetic latitude of $64.1°$, which is statistically a region of the auroral oval. Hence the radar frequently detects nonmeteor targets during substorms associated with ionospheric plasma waves generated due to Farley-Buneman instability (Kelley, 2009). The Doppler velocity of such echoes can be more than a few 100 ms^{-1}, which are mostly detected at low elevation (Lukianova et al., 2018). For the Sodankylä radar, Kozlovsky and Lester (2015) identified
105 ground echoes modulated by the ionosphere during pulsating auroras. These targets have near-zero Doppler velocities, and are also observed at low elevation. Furthermore, the SKiYMET system detects both underdense and overdense echoes as valid meteors. However, more than 95% of detections are underdense (Hocking et al., 2001b). The percentage of overdense trails may be larger during some meteor trails such as Geminids or Quadrantids and this leads to underestimation of temperatures (Kozlovsky et al., 2016). This artefact in temperature was found to be reduced for Sodankylä radar for zenith angle less than
110 $50°$. The initial data selection criteria is kept to bare minimum, such that, all heights and decay times are included as long as they are unambiguous detections above $40°$ elevation angle with Doppler radial velocity in the range $\pm100 \text{ ms}^{-1}$. Subsequently, to

improve the temperature estimation we used a contour selection process, i.e., the data outside certain contour in the normalized height - $log_{10}(1/\tau)$ distribution were rejected (Fig. 1b).

For temperature estimation we considered daily data for a six month period from October 2015 to March 2016 since simultaneous lidar measurements were available during this time. The Compact Rayleigh Autonomous Lidar (CORAL) provided vertical profiles of the atmospheric temperature at 27–98 km over Sodankylä as part of the GW-LCYCLE-II (Gravity Wave Life cycle Experiment) campaign in winter 2015/2016 (Reichert et al., 2019). The median number of daily meteor detections in this data set is 1652, with a minimum of 410 meteor detections on 04 Oct 2015 and a maximum of 3456 detections during the Geminids meteor shower on 14 Dec 2015.

The Mass-Spectrometer-Incoherent-Scatter or MSIS90 (Hedin, 1991) model temperatures are used to generate a temperature gradient model near the peak heights. Model temperatures are computed for each date at intervals of 6 h between 85 km to 95 km. A third-degree polynomial fit is carried out to obtain the height profiles at 6 UT, 12 UT, 18 UT and 24 UT. For each time interval, the gradient at the respective meteor peak height, as well as at 1 km above and below from peak height are estimated. These 12 values are then used to obtain the mean and standard deviation of the temperature gradient for each day near the peak height, which varies in the range 89±1 km. The daily meteor detections, the peak heights, and the corresponding temperature gradient model values are shown in Fig. 2. The standard deviation of the MSIS model values correspond to roughly of the order of 0.7 Kkm^{-1}.

Our reasons for choosing the MSIS temperature gradient are twofold. Firstly, MSIS data are easily accessible from the online version, which guarantees reproducibility of this work independent of location. Secondly, even if the temperature gradient term in Eq. (6) is ignored, the resulting offset in the estimated temperature is on average 10% (Hocking, 1999) or less. Hence an approximate estimate is sufficient for the main objective of this paper. However, the actual temperature gradient in the atmosphere may be slightly different from these model values, which can contribute to the biasing effect in the estimated temperatures. Any such possibility and its effect on the estimated temperatures is addressed in the subsequent section.

3 Method: Regression analysis

3.1 Estimation of error variances in decay time and height

In the following text we use the notation and formulation in Gillard and Iles (2005). The observables, $log_{10}(1/\tau)$ and height, are represented as d_i and h_i respectively, and the corresponding unobserved true values as ξ_i and η_i respectively, where the index i represents the i'th meteor detection. For consistency we also assume that $log_{10}(1/\tau)$ is presented in abscissa and height is in the ordinate in the respective scattered plot (as shown in Fig. 1). Suppose, we are assuming a linear relation in variables ξ_i and η_i as,

$$\eta_i = \alpha + \beta \xi_i, \, i = 1, 2, ..., N \tag{9}$$
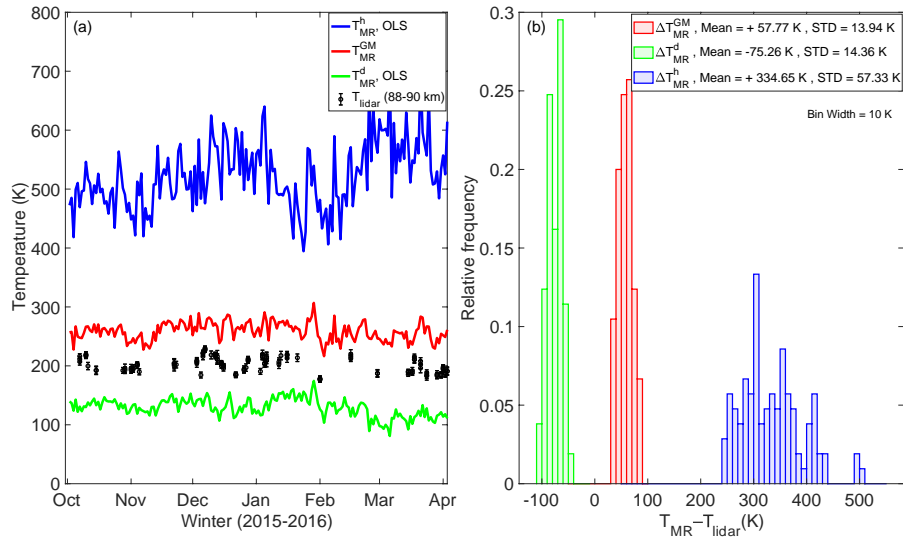
Figure 3. (a) Temperature estimated in OLS method using $log_{10}(1/\tau)$ (*green*) and height (*blue*) as independent variable. Also, showing (*red*) the temperatures obtained using the geometric mean (GM) fitting and the lidar temperatures (in *black*). (b) The offset between the lidar (T_{lidar}) temperatures and the estimated MR temperatures (T_{MR}) using OLS fitting and GM fitting (without contour selection).

Due to measurement errors and various geophysical processes, the true values ξ_i and η_i will be subjected to random errors and hence the observable d_i and h_i will have scatter around the linear model in Eq. (9):

$$d_i = \xi_i + \delta_i \tag{10}$$

145 And,

$$h_i = \eta_i + \varepsilon_i = \alpha + \beta\,\xi_i + \varepsilon_i \tag{11}$$

where δ_i and ε_i are errors in the measured $log_{10}(1/\tau)$ and height respectively, and are assumed to be mutually uncorrelated, have zero mean and independent of the suffix *i*. This implies that the measurement error variances, s_δ and s_ε, are constant with respect to the suffix *i*. Classical regression analysis or ordinary least-squares (OLS) treats d_i as an independent variable

150 without intrinsic errors (or, $d_i = \xi_i$), and then minimises the sum of squared residuals along the ordinate. The slope from the OLS method can be represented in terms of the covariance (Cov) and variance (Var) as (e.g., Smith, 2009; Keles, 2018),

$$\beta_{OLS}^d = \frac{Cov(d_i, h_i)}{Var(d_i)} \equiv r\,\frac{\sqrt{s_h}}{\sqrt{s_d}} \tag{12}$$

where β_{OLS}^d is the OLS slope estimated by considering $log_{10}(1/\tau)$ as independent variable, and r is the Pearson product-moment correlation coefficient between d and h. Likewise, by reversing the arguments above, it's trivial to show that the

155 reciprocal value of OLS slope estimate with height as independent variable is (e.g., Smith, 2009),

$$\beta_{OLS}^h = \frac{Var(h_i)}{Cov(d_i, h_i)} \equiv \frac{1}{r}\,\frac{\sqrt{s_h}}{\sqrt{s_d}} \tag{13}$$

To see the effect of errors in the independent variable on the OLS slope estimate, e.g., for β^d_{OLS}, Eq. (10) and Eq. (11) are used in Eq. (12),

$$\beta^d_{OLS} = \frac{Cov(\xi_i + \delta_i, \alpha + \beta\,\xi_i + \varepsilon_i)}{Var(\xi_i + \delta_i)} \tag{14}$$

160 Since δ_i, ε_i and ξ_i are mutually independent, Eq. (14) simplifies to,

$$\beta^d_{OLS} = \frac{\beta\,Cov(\xi_i, \xi_i)}{Var(\xi_i + \delta_i)} = \frac{1}{1 + \frac{Var(\delta_i)}{Var(\xi_i)}}\,\beta = \zeta\,\beta \tag{15}$$

where ζ is known as the *attenuation* or *regression dilution bias*. Since variances are always positive by definition, Eq. (15) shows that in the presence of measurement error in the so-called independent variable (in abscissa), the OLS slope estimate (β^d_{OLS}) will always be smaller than the unbiased slope β. Likewise, β^h_{OLS} is greater than β if there is error in the measured

165 height (specific example presented in Fig. 1a). By substituting $d_i = \xi_i + \delta_i$, Eq. (15) can be rearranged as

$$\beta^d_{OLS} = (1 - \frac{Var(\delta_i)}{Var(d_i)})\,\beta \tag{16}$$

Equation (16) is a well known identity in statistical literature (e.g., Carroll and Ruppert, 1996; Frost and Thompson, 2000), that was re-derived by Hocking et al. (2001b) in Eq. (7) in the context of SCT correction. Equation (16) reveals that an absolute knowledge of error variances, s_δ (or s_ε), is required to obtain the bias-corrected slope (β) if we choose OLS fitting for the

170 slope estimate. A common practice is to calibrated the biased slope with optical or satellite data by arbitrarily choosing a value of s_δ or s_ε (e.g., Holdsworth et al., 2006; Hocking et al., 2007; Kim et al., 2012). In the remaining part of this section, we demonstrate how to obtain an average value of the error variances in this data following a revised calibration procedure.

For each 24 h of the data set, we performed two OLS fittings to estimate β^d_{OLS} and β^h_{OLS} by using Eq. (12) and Eq. (13). The corresponding biased temperatures, T^d_{MR} and T^h_{MR} respectively, are estimated using Eq. (6). Experimental values of the

175 parameters s_δ and s_ε can be obtained by comparing these estimated biased temperatures with the colocated lidar temperatures (T_{lidar}) as the reference values. Using Eq. (7) and Eq. (8), and noting that the slope is proportional to the estimated temperatures from Eq. (6) we obtain:

$$s_\delta \approx (\frac{T_{lidar} - T^d_{MR}}{T_{lidar}})\,s_d \text{ and } s_\varepsilon \approx (\frac{T^h_{MR} - T_{lidar}}{T^h_{MR}})\,s_h \tag{17}$$

where T^d_{MR} and T^h_{MR} are MR temperatures estimated using OLS fitting with $log_{10}(1/\tau)$ and height as independent variable

180 respectively. Furthermore, if the measurements are normalised with the mean and standard deviation (STD) as

$$d'_i = \frac{d_i - mean(d_i)}{\sqrt{s_d}} \text{ and } h'_i = \frac{h_i - mean(h_i)}{\sqrt{s_h}} \tag{18}$$

then, $Var(d'_i) = Var(h'_i) = 1$, and the OLS estimate of the ratio of the measurement error variance is (from Eq. (17) and Eq. (18)):

$$\lambda^{OLS}_{eff} = \frac{s_{\varepsilon'}}{s_{\delta'}} \approx \frac{T^h_{MR} - T_{lidar}}{T_{lidar} - T^d_{MR}} \cdot \frac{T_{lidar}}{T^h_{MR}} \tag{19}$$

185 where the error variances, $s_{\varepsilon'}$ and $s_{\delta'}$, are in the dimension free system defined by Eq. (18). In essence, λ_{eff}^{OLS} is a measure of all sources of errors in the normalised heights and decay times that cause the real data to deviate from the idealized physical model of Eq. (6), thereby producing a typical scatter as seen in Fig. 1.

  λ_{eff}^{OLS}, s_{δ}, and s_{ε} were estimated by Eq. (17) and Eq. (19) using 24 h of MR data and colocated lidar temperatures at 88 km, 89 km and 90 km for the dates for which lidar data was available. The biasing effect on the OLS estimate of MR temperatures

190 with $log_{10}(1/\tau)$ and height as independent variable respectively are presented in Fig. 3 (green and blue lines and histogram). As expected from Eq. (7) or Eq. (8), a mean offset of -75 K and +335 K occurs depending on whether $log_{10}(1/\tau)$ or height respectively is considered as independent variable. In practice, the magnitude of these biases is related to the total errors in heights and $log_{10}(1/\tau)$ from Eq. (17), which was not taken into account by the OLS regression model in Eq. (12) and Eq. (13). Furthermore, the relative density contour lines for each data point is obtained by counting the number of detections in

195 a circle of unit area in the normalised height-$log_{10}(1/\tau)$ plane relative to the number of detections in unit area at the peak meteor region (Fig. 1b). In addition, all the error estimates from SCT method are obtained at contour levels 0, 0.2 and 0.4, and the results are presented in Table 1. Several key features of these data are reflected in Table 1. Despite the data transformation via Eq. (18), the average error variances for the height data are more than those for the $log_{10}(1/\tau)$ data in these coordinates. This asymmetry in the error variances implies that the bivariate distribution is slightly skewed away from a perfectly normal

200 distribution along the Y-direction. However, this effect of asymmetric error variances is less pronounced near the core of this distribution. This implies that the parameter λ_{eff}^{OLS} is closer to 1 near the core of this distribution and further away from 1 near the tail of the distribution. The data near the outer contour area is subjected to larger parameter estimation error due to observational limitation. For example, the zenith angle dependent error in height can easily skew the distribution in this direction. On the other hand, natural geophysical variability in these data contributes significantly at all altitudes. As seen in

205 Table 1, the average error in height for contour levels 0, 0.2 and 0.4 are 5.0 km, 3.0 km and 2.2 km respectively. This error is significantly higher than what is expected from purely parameter estimation error (for zenith angle less than $50°$, the error in height is 1 km or less), indicating that geophysical variability dominates the total error variance in these data at all altitudes. The average error variances estimated at the contour level 0.2 (Table 1) correlate very well with the values reported in Hocking (2004) and Holdsworth et al. (2006). Hocking (2004) estimated $\triangle(height) = 3.25$ km using a numerical model for a pulse length equivalent to 2 km, and a meteor at an altitude of 90 km and zenith angle $50°$. Likewise, their estimation of $\triangle log_{10}(1/\tau) =$

210 0.14 was based on simulation studies for meteors below 95 km and confirmed that 'decay-times variability' arise due to 27% variability in K_{amb} and 8% variability in temperatures over meteor region. The argument for choosing 95 km as the maximum height is that above this altitude meteor decay rates are substantially affected by processes other than ambipolar diffusion. Holdsworth et al. (2006, p 5) applied similar data rejection criteria and found out that $\triangle log_{10}(1/\tau) = 0.14$ is required to

215 calibrate the slope if $log_{10}(1/\tau)$ is used as independent variable in the OLS regression model. Likewise, Thorsen et al. (1997) performed the comparison between the parameter estimation error and the geophysical variability for estimating the mean wind field in the middle atmosphere, and found that the geophysical variability dominated at all heights.

  It is worth noting that instead of directly using the individual observation between biased MR temperatures and lidar measurements from Eq. (17), we have used the statistical mean of differences for calibration. This is because lidar data is not

Table 1. The average value of the (square root of) error variances in height and $log_{10}(1/\tau)$, $s_{\varepsilon'}$ and $s_{\delta'}$ are given along with the average value of λ from SCT calibration (λ_{eff}^{OLS}) at contour levels 0, 0.2 and 0.4 for winter 2015–2016.

Contour:	0	0.2	0.4
$\sqrt{s_{\varepsilon}}/km$	5.0	3.0	2.2
$\sqrt{s_{\delta}}/s^{-1}$	0.18	0.14	0.11
$<s_{\varepsilon'}>$	0.62	0.44	0.38
$<s_{\delta'}>$	0.37	0.31	0.30
$<\lambda_{eff}^{OLS}>$	1.68	1.43	1.25

available for all days during the 6 months of data used in this work. Moreover, both MR and lidar data have their own intrinsic errors and technical differences in the observation time and volume of sky. MR temperatures are daily averages over 24 h of observation, whereas lidar data is just the nightly mean profile. The lidar probes a small volume limited to the diameter of the lidar beam, while the radar illuminates a large part of the sky. For a *single* observation, the lidar may see the phase structure of large-scale gravity waves while the MR averages over the gravity wave structure due to different spatial resolutions. As a result, the radar averages over gravity waves with horizontal wavelengths smaller than few hundred km. On the other hand, the lidar may resolve these gravity waves if the run time is shorter than the period of these waves. As gravity wave amplitudes can be upto 10–15 K at these altitudes (Reichert et al., 2019), we cannot expect perfect agreement between radar and lidar temperature due to geophysical variation which shows up differently in the two data sets as a result of the different observational volumes.

While such calibration routine may prevent large offsets in the estimated temperatures, the day-to-day variation in these error variances due to natural geophysical processes will persistently introduce artefacts in the estimated temperatures. Moreover, due to the continually changing atmospheric dynamic, these calibration parameters need to be updated at time intervals. This in turn requires availability of optical or satellite data throughout the year for the given location. In all generality, it is desirable to avoid any kind of calibration process and instead formulate an independent estimate of temperatures using MR data alone. As an alternative to the OLS method, Errors-in-Variables (EIV) regression analysis provides a way to incorporate the error variances in both height and $log_{10}(1/\tau)$ data thereby reducing the biasing effect in the estimated slope parameter.

3.2 Errors-in-Variables (EIV) model: GM solution

For fitting a straight line model, such as,

$$y(x) = a + bx \tag{20}$$

to a set of N data points (x_i, y_i) measured with errors, the corresponding χ^2 merit function is (Press et al., 1992, p 660)

$$\chi^2 = \sum_{i=1}^{N} \frac{(y_i - a - bx_i)^2}{\sigma_{yi}^2 + b^2 \sigma_{xi}^2} \tag{21}$$

where σ_{yi} and σ_{xi} are the standard deviation of the i'th data point, and the weighted sum in the denominator of Eq. (21) can be interpreted as the weighted-error of the i'th data point. The regression coefficients, a and b, can be found by minimising

the merit function with respect to these coefficients following any suitable numerical root-finding routine. However, under the assumption of symmetric error variances, it is possible to derive an analytic solution for the regression coefficients. This

245   solution, when the data is appropriately normalised, leads to a slope estimate which is both scale-invariant and symmetric with respect to the data.

Application of Eq. (21) to physics data requires that all measured variables are dimensionally consistent so that χ^2 is dimension free. Moreover, the analysis in this section requires that the measurements are presented in an appropriate dimension free system. This facilitate the direct comparison between different parameters, such as, the measured variables or the associated

250   error variances. By applying the coordinate transformation introduced in Eq. (18) to Eq. (9), we therefore intend to solve the simplified bivariate linear system of equations,

$$\eta_i' = \beta \, \frac{\sqrt{s_d}}{\sqrt{s_h}} \, \xi_i' \equiv \beta_W \, \xi_i' \tag{22}$$

where η_i', ξ_i' and β_W are dimension free. For the specific choice of normalisation by Eq. (18), the intercept (α_W) is always zero in the transformed coordinate system. The merit function in Eq. (21) can be further simplified by invoking a *homoscedastic*

255   *standard weighting model* (Macdonald and Thompson, 1992). This error model assumes that the error variances are independent of data point, thereby simplifying the merit function as (Macdonald and Thompson, 1992; Lolli and Gasperini, 2012),

$$\chi^2(\beta_W, \alpha_W = 0) \equiv \sum_{i=1}^{N} \frac{(h_i' - \beta_W d_i')^2}{s_{\delta'} (\lambda + \beta_W^2)} \tag{23}$$

where $s_{\delta'}$ and $s_{\varepsilon'}$ are *constant* error variances of the measured $log_{10}(1/\tau)$ and heights respectively in the normalised (or,

260   dimension free) coordinate system, and λ is the ratio

$$\lambda = \frac{s_{\varepsilon'}}{s_{\delta'}} \tag{24}$$

The χ^2 minimisation of Eq. (23) with respect to β_W leads to the analytic expression (Carroll and Ruppert, 1996; Smith, 2009; Lolli and Gasperini, 2012) for the EIV slope parameter in terms of the variances ($s_{d'}$, $s_{h'}$) and covariances ($s_{h'd'}$) of the measured variables,

265   $$\beta_W = \frac{s_{h'} - \lambda s_{d'} + \sqrt{(s_{h'} - \lambda s_{d'})^2 + 4\lambda s_{h'd'}^2}}{2s_{h'd'}} \tag{25}$$

Or,

$$\beta_W \equiv \frac{1 - \lambda + \sqrt{(1 - \lambda)^2 + 4\lambda s_{h'd'}^2}}{2s_{h'd'}} \tag{26}$$

Since $s_{d'} = s_{h'} = 1$ from Eq. (18). And the covariance ($s_{h'd'}$) is computed using the standard definition,

$$s_{h'd'} = \frac{1}{N} \sum_{i=1}^{N} (h_i' d_i'), \text{ for large } N \tag{27}$$

270   Equation (26) can be solved if a prior knowledge of λ is available, which in turn requires a precise estimate of all sources of errors in the measured data. In the more practical case for unknown λ, we need to initiate a good starting estimate. Using the calibration procedure described by Eq. (17) and Eq. (18), the mean values of $s_{\varepsilon'}$ and $s_{\delta'}$ are found to be 0.62 ± 0.04 and 0.37 ± 0.06 respectively (without any contour selection: Table 1). Since the EIV estimate of the slope requires only the ratio between $s_{\varepsilon'}$ and $s_{\delta'}$, a good choice of this starting value is $\lambda = 1$. Furthermore, for $\lambda = s_{\varepsilon'} = s_{\delta'} = 1$, there exists a simple

275 geometric interpretation of the merit function in Eq. (23). This solution corresponds to minimising the euclidean or orthogonal distance between the fitted line and the measured data. The residual function to be minimised with respect to the regression coefficients is

$$\chi^2 = \sum_{i=1}^{N} \frac{(h_i' - \beta_W d_i')^2}{1 + \beta_W^2} \equiv \sum_{i=1}^{N} \frac{(h_i' - d_i')^2}{2} \qquad (28)$$

since $\beta_W = 1$ when $\lambda = 1$ from Eq. (26). Following Eq. (22), we therefore have our *first estimate* of β in the scattered plot of

280 $log_{10}(1/\tau)$ and heights,

$$\beta = \frac{\sqrt{s_h}}{\sqrt{s_d}} \qquad (29)$$

Equation (29) is commonly referred to as reduced major axis (RMA) solution in statistics literature (Smith, 2009). In practice, this is just the geometric mean (GM) of the two OLS estimates, β_{OLS}^d and β_{OLS}^h, as can be seen by combining Eq. (12) and Eq. (13),

285 $$\beta_{GM} = \sqrt{\beta_{OLS}^d \, \beta_{OLS}^h} \equiv \frac{\sqrt{s_h}}{\sqrt{s_d}} \qquad (30)$$

The GM solution in Eq. (30) has the unique feature that this is the only case of EIV estimate which is both scale-invariant and symmetric in the variables (e.g., Ricker, 1984; Smith, 2009). While these properties do not necessarily imply that the GM solution is the correct solution (discussed below), but this *first estimate* reflects the nature of biasing effect in the estimated slope in relation to the data selection process. A specific example of GM fitting is presented in Fig. 1a. The standard error in

290 the OLS and GM slope estimate reported in Fig. 1a follows from Vicente de Julia´n-Ortiz et al. (2010). Due to the relatively low detections with Sodankylä radar (Fig. 2c), the 2-sigma error in the estimated temperature using GM solution is found to be significantly higher (13 K on average at contour level 0). This 13 K of noise level in the temperature can be reduced by a factor of $\sqrt{3}$ or $\sqrt{5}$ if a 3-day or 5-day running mean of temperature is estimated with this radar. However, to test the robustness of the proposed method, this paper has estimated the daily averaged temperatures.

295   The systematic offset between MR temperature and colocated lidar temperature as a result of using Eq. (30) is reflected in Fig. 3a (red curve) and Fig. 3b (red histogram). Each of these temperatures are then compared with lidar temperatures at 88 km, 89 km and 90 km for the dates when lidar data are available. The intrinsic noise in the lidar temperature is about 5–10 K (Reichert et al., 2019), which implies no temperature gradient is observed between 88–91 km in these data. Figure 3b (red histogram) reveals that the MR temperatures are over-estimated by a mean value of +58 K for the case of GM solution .

300   When compared to the temperature-gradient model derived from optical, satellite and rocket climatology (e.g., Holdsworth et al., 2006), it can be easily argued that our MSIS-derived gradient model (Fig. 2a) is more negative than expected. If these

values are shifted by a constant positive offset of +1 Kkm^{-1}, the absolute value of the estimated temperatures will increase by 10 K (Singer et al., 2004). This will further increase the offset between lidar and MR temperature, thereby shifting the histogram (in red) in Fig. 3b further to the right.

305   On the other hand, lidar temperatures are usually obtained during the night time, which can lead to a systematic offset due to day-night differences or tidal variations. As discussed by Hocking et al. (2004), the day-night temperature difference at these altitudes is of the order of 3–4 K. This is significantly less than the standard errors in these temperatures, which is on average 6 K at contour level 0. Hence we expect the day-night difference in Sodankylä MR temperatures to be insignificant during the winter period. Moreover, any attempt to estimate MR temperatures using only night-time data has the adverse effect of reducing

310   the accuracy in the estimated temperatures due to data loss. While no specific studies of tidal variation have been made for this location, the data from other sites (e.g., Hocking and Hocking, 2002; Stober et al., 2008) show that the temperature variation due to tidal activity is typically less than 10 K. We can therefore rule out the possibility of an offset in the MSIS gradient model or tidal effects as the primary cause for the +58 K offset seen in Fig. 3b (red histogram).

      Ricker (1984) emphasised that the biasing in GM solution is conditional upon the value of the correlation coefficient (r)

315   between the variables, while Kimura (1992) demonstrated that this solution will be an overestimate in the case of low r value. For the data set used in this work, we found that the correlation between $log_{10}(1/\tau)$ and height is typically 0.50 ± 0.05, thereby indicating the presence of significant natural variation in the measurements. Furthermore, Jolicoeur (1990) used error modelling to conclude that r must be more than 0.6 for the the GM solution to be acceptable. In fact, we have observed that if we restrict our data selection process by excluding all data beyond the density contour 0.2 (Fig. 1b), this increases the r to

320   be typically around 0.66 ± 0.06 with the consequence of reduced biasing in the GM solution. Such contour selection process essentially removes the erroneous data at higher and lower altitudes from the tail of the distribution, whereby the assumption of equal error variances (i.e., $s_{\varepsilon'} \approx s_{\delta'}$) is achieved in the normalised coordinates (Table 1). In other words, the validity of GM solution is conditional upon how close the parameter λ is to 1 for a given data selection process.

4   Results and Discussion

325   The convergence of λ towards 1 near the core of this bivariate distribution is evident from Table 1. This is demonstrated in Fig 4a, where we have estimated the GM slope at various contour levels between 0 to 0.7. In addition, Fig 4b reflects the asymptotic behaviour of GM solution at higher contour levels in normalised coordinates. For these data, beyond the contour level 0.4, any change in slope at higher contour level is within the 2-sigma error limit. This error in the slope corresponds to an average 2–sigma error of 11 K in the estimated temperatures at contour level 0.4. In addition, the estimated temperatures can

330   be biased due to small variation of λ from 1 on a day-by-day basis. For example, If the true value of λ is 1.25, the GM slope will be overestimated by 4% (from Eq. (26) for the date 14 Nov 2015). For a typical winter temperature of 200 K at 90 km, a 4% offset translates to overestimation of temperatures by 8 K. In principle, this bias can be further reduced by selecting a higher contour level than 0.4 with the consequence of increased noise level in the estimated temperatures. For these data, the
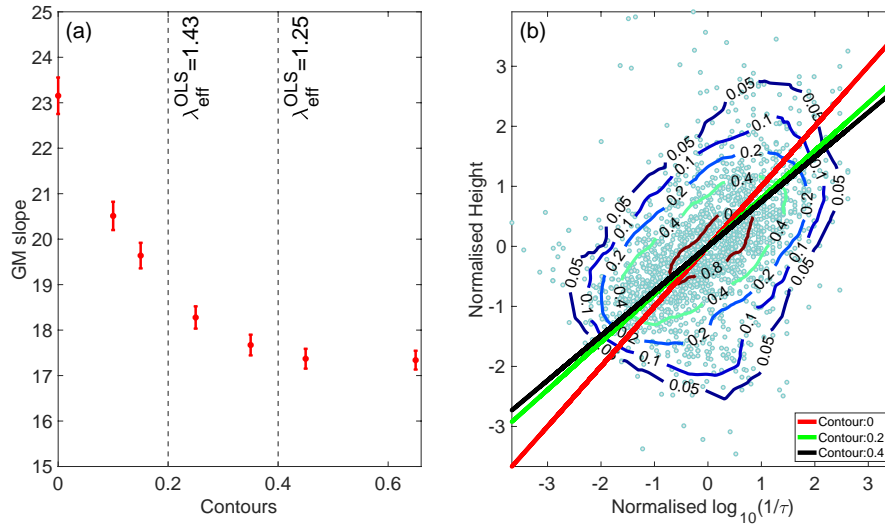
Figure 4. GM solution at different contour levels in (a) original coordinate and in (b) normalised coordinate for the date 14 Nov 2015. The vertical dashed lines in (a) correspond to the average value of λ obtained from SCT calibration at contour level 0.2 and 0.4 respectively for winter 2015–2016. The error bar in (a) corresponds to 2×standard error.
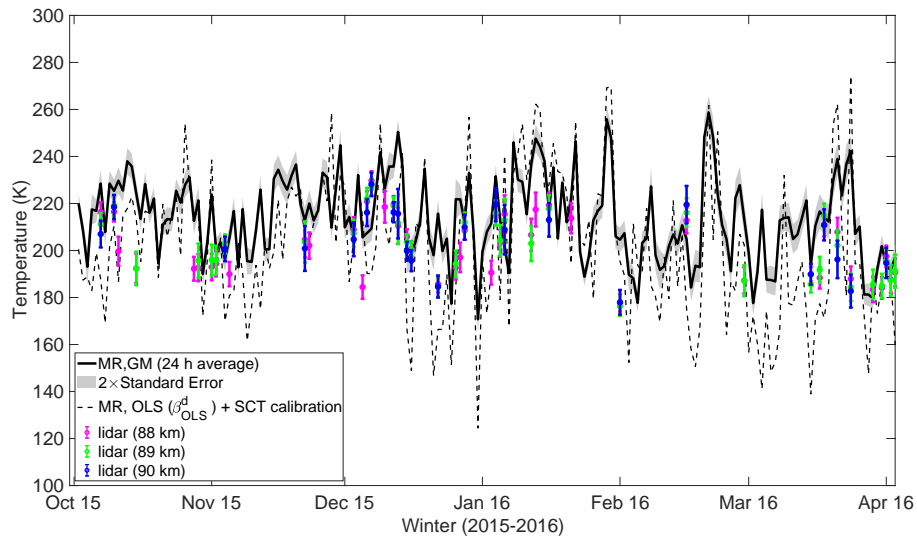
Figure 5. Comparison of the bias-corrected MR temperatures with lidar data for the winter 2015–2016. The *solid* line corresponds to the temperature estimated using the GM solution at contour level 0.4. The *dashed* line corresponds to the SCT calibrated temperatures using the colocated lidar measurements. The OLS estimates are obtained with $log_{10}(1/\tau)$ as independent variable. The errors in lidar temperatures are 5–10 K and the 2-sigma error (grey shade) of the temperature from EIV analysis is on average 11 K. The differences between lidar and MR temperatures are presented in Fig. 6.
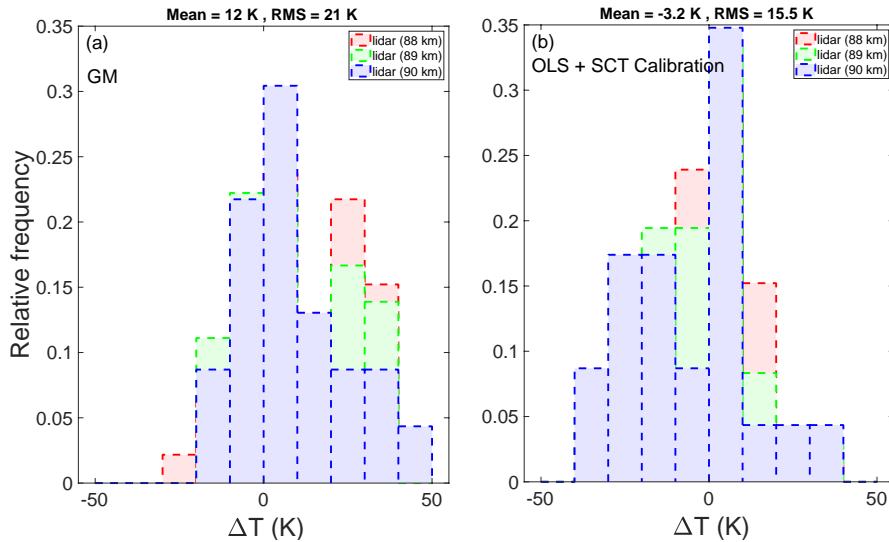
Figure 6. Difference between MR temperatures and lidar data for (a) GM solution at contour level 0.4 and (b) SCT calibration applied to OLS estimate of β_{OLS}^{d}. MR temperatures are shown in Fig. 5.

contour level 0.4 is found to provide an optimum condition such that a maximum of 25% uncertainty in the parameter λ leads
335 to 4% bias in temperature which, in turn, is comparable to the standard error in the temperature from regression analysis.

We have applied the GM slope estimate at contour level 0.4 to the MR data from the period October 2015 to March 2016. This is presented in Fig. 5, along with the data from colocated lidar observations. The differences between MR temperatures and lidar are shown in Fig. 6a for altitudes near peak meteor counts. The mean difference between lidar and MR temperatures is +12 K which is expected due to the variation in the true value of λ from 1. The root-mean-square differences (RMS) is about
340 21 K. This difference is partly due the intrinsic errors of 5–10 K in lidar temperature and partly due to the statistical noise in the estimated MR temperatures.

For direct comparison with the results above, we have also estimated the MR temperatures using the revised SCT calibration procedure described in Sect. 3.1. For this we have estimated the OLS slope (β_{OLS}^{d}) and used $\sqrt{s_{\delta}} = 0.11$ (Table 1) to obtain the calibrated temperatures from Eq. (16) and Eq. (6). These calibrated temperatures are presented in Fig. 5. The histogram
345 in Fig. 6b shows the differences between lidar data and the SCT calibrated MR temperatures. The mean difference between the MR and lidar temperatures is again about -3 K, thereby showing that the biasing effect has been properly corrected by this calibration procedure. The RMS difference is 15 K. Although the temperature estimated from the GM solution is slightly biased as compared to that estimated using SCT calibration, the presence of artefacts in the latter is clearly visible in Fig. 5. As evident from Fig. 7, the GM solution based on contour selection improves the temperature estimation significantly as compared
350 to the traditional use of the OLS regression analysis.

The EIV analysis does not distinguish between the measurement error and natural geophysical variability (e.g., Sprent, 1990, p 13). In other words, the error variances, $s_{\delta'}$ and $s_{\varepsilon'}$, consist of both measurement errors and the natural geophysical variation.
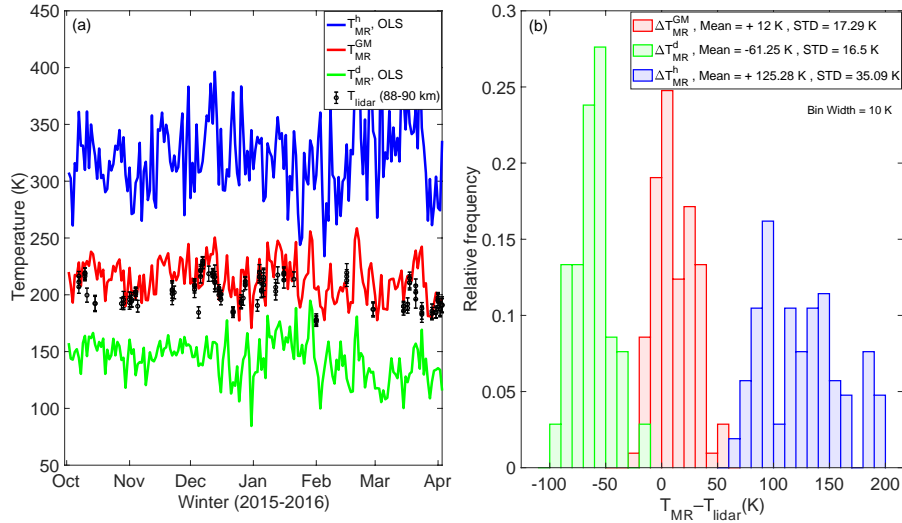
Figure 7. (a) Improved temperature estimation using GM solution (red) as compared to OLS estimates (blue and green) at contour level 0.4. (b) Reduced mean offset between MR and lidar temperature for GM slope estimate (red) as compared to OLS estimate (green and blue).

The effective value of λ in a normalised coordinate may vary on a day-by-day basis and may be radar dependent. For example, meteor trails can get modified by wind effects, ion composition, meteor fragmentation, strong ionospheric currents as well as temperature and pressure fluctuations on various spatial and temporal scales (Hocking, 2004; Younger et al., 2014). Despite the contour selection process, asymmetric effects of geophysical variation may have increased the effective variance of h_i' leading to overestimate in the GM solution (Gillard and Iles, 2005). Due to the high-latitude location of Sodankylä radar, geomagnetic effect above 95 km can contribute to the systematic bias. Below 85 km, the decay of meteor radar echoes may deviate slightly from diffusion-only evolution (Lee et al., 2013) thereby requiring a better physical model that doesn't assume the linearity of Eq. (6). Assessing the contribution of geophysical variability at various altitudes would require carefully designed replicates of observations as well as long term comparison of MR temperatures with other colocated instruments. In other words, the case for $\lambda \neq 1$ need to be handled with careful modelling of errors by taking into account the dominant effect of geophysical variability in these data. This remains a subject of future research.

5 Summary

The biasing effect in MR temperature has been a pressing issue for the last two decades. Attempts have been made in the past to correct the slope in the scattered plot of $log_{10}(1/\tau)$ and height, usually either by direct calibration with optical or satellite data or by an arbitrary choice of data rejection criteria to exclude parts of measurements. This paper has addressed the underlying reasons for such biasing effect, which is mainly due to the presence of various error terms. We have reviewed the conventional calibration procedure (1), and then provided an alternative method (2) for estimating MR temperature that doesn't require any

370 calibration. We have applied both of these methods to the MR data from winter 2015–2016, and assessed the quality of the estimated MR temperature using colocated lidar measurements. The key points from each of these two aspects of the paper are given below.

1. This paper has reviewed the *statistical comparison technique* (SCT), originally proposed by Hocking et al. (2001b), within the context of MR temperature calibration. We have extended the theoretical basis of the SCT method to obtain an estimate of error variances of $log_{10}(1/\tau)$ and height using colocated lidar measurements. No significant offset was seen in the calibrated MR temperature, even without applying any outlier rejection criteria. But artefacts introduced due to the difference in measurement techniques between MR and lidar were clearly visible in the estimated temperatures.

2. As an alternative method, we have applied the *Errors-in-Variables* (EIV) regression analysis to estimate the slope in the scattered plot of $log_{10}(1/\tau)$ and height. The model error in EIV analysis takes into account the total errors variances in both abscissa and ordinate. It is observed that the geophysical variability dominates at all altitudes as compared to measurement errors and is the key factor in addressing the biasing effect. Moreover, any asymmetry in the error variance is minimal near the meteor peak region. This allows an independent estimate of weighted-averaged atmospheric temperatures at 90 km using a suitable contour selection procedure. The temperatures estimated using this method show very good agreement with colocated lidar measurement, and with reduced systematic offset as compared to the traditional least-square analysis.

Data availability. The meteor radar data were collected at SGO (https://www.sgo.fi/Projects/SLICE/). Data used in the paper are available at https://www.sgo.fi/pub/AMT_2020_ESarkar/. The MSIS model data were obtained from https://ccmc.gsfc.nasa.gov/modelweb/. The lidar data are available at https://halo-db.pa.op.dlr.de/mission/109.

Author contributions. ES developed the method, carried out all data analysis and wrote the manuscript. The idea was suggested by AK, who also supervised this work. TU prepared the script for reading the raw data files from the radar, and supervises the doctoral thesis of ES. IV co-supervises the doctoral thesis of ES and made suggestions. BK provided the lidar data. ML supported the MR operation at the Sodankylä. All the authors contributed to proof reading the manuscript.

Competing interests. no competing interests are present

Acknowledgements. ES thanks the University of Oulu's Kvantum Institute for their support. IV acknowledges support from the Academy of Finland, project 301542. BK acknowledges support of the German Research Foundation (DFG), research unit Multiscale Dynamics of

Gravity Waves (MS-GWaves) grant RA 1400/6-1. ML acknowledges support from the Science and Technologies Facilities Council (STFC) grant ST/S000429/1. We thank the anonymous referees for providing helpful suggestions to improve this manuscript.

References

Bronshten, V. A.: Physics of meteoric phenomena, Dordrecht, Holland: Kluwer, 1983.

400 Carroll, R. and Ruppert, D.: The use and misuse of orthogonal regression in linear errors-in-variables models, The American Statistician, 50, 1–6, https://www.tandfonline.com/doi/abs/10.1080/00031305.1996.10473533, 1996.

Chilson, P. B., Czechowsky, P., and Schmidt, G.: A comparison of ambipolar diffusion coefficients in meteor trains using VHF radar and UV lidar, Geophysical research letters, 23, 2745–2748, https://doi.org/10.1029/96GL02577, 1996.

Frost, C. and Thompson, S. G.: Correcting for regression dilution bias: comparison of methods for a single predictor variable, Journal of the
405 Royal Statistical Society: Series A (Statistics in Society), 163, 173–189, https://doi.org/10.1111/1467-985X.00164, 2000.

Gillard, J. W. and Iles, T. C.: Method of moments estimation in linear regression with errors in both variables, Cardiff University School of Mathematics Technical Paper, 2005.

Hedin, A. E.: Extension of the MSIS thermosphere model into the middle and lower atmosphere, Journal of Geophysical Research: Space Physics, 96, 1159–1172, https://doi.org/10.1029/90JA02125, 1991.

410 Hocking, W. K.: Temperatures using radar-meteor decay times, Geophysical Research Letters, 26, 3297–3300, https://doi.org/10.1029/1999GL003618, 1999.

Hocking, W. K.: Radar meteor decay rate variability and atmospheric consequences, Annales Geophysicae, 22, 3805–3814, https://doi.org/10.5194/angeo-22-3805-2004, 2004.

Hocking, W. K. and Hocking, A.: Temperature tides determined with meteor radar, Annales Geophysicae, 20, 1447–1467, https://hal.
415 archives-ouvertes.fr/hal-00317146, 2002.

Hocking, W. K., Thayaparan, T., and Jones, J.: Meteor decay times and their use in determining a diagnostic meso-spheric temperature-pressure parameter: Methodology and one year of data, Geophysical Research Letters, 24, 2977–2980, https://doi.org/10.1029/97GL03048, 1997.

Hocking, W. K., Fuller, B., and Vandepeer, B.: Real-time determination of meteor-related parameters utilizing modern digital technology,
420 Journal of Atmospheric and Solar-Terrestrial Physics, 63, 155–169, https://doi.org/10.1016/S1364-6826(00)00138-3, 2001a.

Hocking, W. K., Thayaparan, T., and Franke, S. J.: Method for statistical comparison of geophysical data by multiple instruments which have differing accuracies, Advances in Space Research, 27, 1089–1098, https://doi.org/10.1016/S0273-1177(01)00143-0, 2001b.

Hocking, W. K., Singer, W., Bremer, J., Mitchell, N., Batista, P., Clemesha, B., and Donner, M.: Meteor radar temperatures at multiple sites derived with SKiYMET radars and compared to OH, rocket and lidar measurements, Journal of Atmospheric and Solar-Terrestrial
425 Physics, 66, 585–593, https://doi.org/10.1016/j.jastp.2004.01.011, 2004.

Hocking, W. K., Argall, P. S., Lowe, R. P., Sica, R. J., and Ellinor, H.: Height-dependent meteor temperatures and comparisons with lidar and OH measurements, Canadian journal of physics, 85, 173–187, https://doi.org/10.1139/p07-038, 2007.

Holdsworth, D. A., Morris, R. J., Murphy, D. J., Reid, I. M., Burns, G. B., and French, W. J. R.: Antarctic mesospheric temper-ature estimation using the Davis mesosphere-stratosphere-troposphere radar, Journal of Geophysical Research: Atmospheres, 111,
430 https://doi.org/10.1029/2005JD006589, 2006.

Jolicoeur, P.: Bivariate allometry: interval estimation of the slopes of the ordinary and standardized normal major axes and structural rela-tionship, Journal of Theoretical Biology, 144, 275–285, https://doi.org/10.1016/S0022-5193(05)80326-1, 1990.

Jones, J.: On the decay of underdense radio meteor echoes, Monthly Notices of the Royal Astronomical Society, 173, 637–647, https://doi.org/10.1093/mnras/173.3.637, 1975.

Jones, W.: Theory of diffusion of meteor trains in the geomagnetic field, Planetary and space science, 39, 1283–1288, https://doi.org/10.1016/0032-0633(91)90042-9, 1991.

Kaiser, T.: Radio echo studies of meteor ionization, Advances in Physics, 2, 495–544, https://doi.org/10.1080/00018735300101282, 1953.

Keles, T.: Comparison of Classical Least Squares and Orthogonal Regression in Measurement Error Models, International Online Journal of Educational Sciences, 10, https://doi.org/10.15345/iojes.2018.02.0103.014, 2018.

Kelley, M. C.: The Earth's ionosphere: plasma physics and electrodynamics, Academic press, 2009.

Kim, J.-H., Kim, Y. H., Jee, G., and Lee, C.: Mesospheric temperature estimation from meteor decay times of weak and strong meteor trails, Journal of atmospheric and solar-terrestrial physics, 89, 18–26, https://doi.org/10.1016/j.jastp.2012.07.003, 2012.

Kimura, D. K.: Symmetry and scale dependence in functional relationship regression, Systematic biology, 41, 233–241, https://doi.org/10.1093/sysbio/41.2.233, 1992.

Kozlovsky, A. and Lester, M.: On the VHF radar echoes in the region of midnight aurora: Signs of ground echoes modulated by the ionosphere, Journal of Geophysical Research: Space Physics, 120, 2099–2109, https://doi.org/10.1002/2014JA020715, 2015.

Kozlovsky, A., Lukianova, R., Shalimov, S., and Lester, M.: Mesospheric temperature estimation from meteor decay times during Geminids meteor shower, Journal of Geophysical Research: Space Physics, 121, 1669–1679, https://doi.org/10.1002/2015JA022222, 2016.

Lee, C. S., Younger, J. P., Reid, I. M., Kim, Y. H., and Kim, J.-H.: The effect of recombination and attachment on meteor radar diffusion coefficient profiles, Journal of Geophysical Research: Atmospheres, 118, 3037–3043, https://doi.org/10.1002/jgrd.50315, 2013.

Lolli, B. and Gasperini, P.: A comparison among general orthogonal regression methods applied to earthquake magnitude conversions, Geophysical Journal International, 190, 1135–1151, https://doi.org/10.1111/j.1365-246X.2012.05530.x, 2012.

Lukianova, R., Kozlovsky, A., and Lester, M.: Recognition of meteor showers from the heights of ionization trails, Journal of Geophysical Research: Space Physics, 123, 7067–7076, https://doi.org/10.1029/2018JA025706, 2018.

Macdonald, J. R. and Thompson, W. J.: Least-squares fitting when both variables contain errors: Pitfalls and possibilities, American Journal of Physics, 60, 66–73, https://doi.org/10.1119/1.17046, 1992.

Press, W. H., Teukolsky, S. A., Flannery, B. P., and Vetterling, W. T.: Numerical recipes in Fortran 77: volume 1, volume 1 of Fortran numerical recipes: the art of scientific computing, Cambridge university press, 1992.

Reichert, R., Kaifler, B., Kaifler, N., Rapp, M., Pautet, P.-D., Taylor, M. J., Kozlovsky, A., Lester, M., and Kivi, R.: Retrieval of intrinsic mesospheric gravity wave parameters using lidar and airglow temperature and meteor radar wind data, Atmospheric Measurement Techniques, 12, 5997–6015, https://doi.org/10.5194/amt-12-5997-2019, 2019.

Ricker, W. E.: Computation and uses of central trend lines, Canadian Journal of Zoology, 62, 1897–1905, https://doi.org/10.1139/z84-279, 1984.

Robson, R. E.: Dispersion of meteor trails in the geomagnetic field, Physical Review E, 63, 026 404, https://doi.org/10.1103/PhysRevE.63.026404, 2001.

Singer, W., Bremer, J., Weiß, J., Hocking, W. K., Höffner, J., Donner, M., and Espy, P.: Meteor radar observations at middle and Arctic latitudes Part 1: mean temperatures, Journal of atmospheric and solar-terrestrial physics, 66, 607–616, https://doi.org/10.1016/j.jastp.2004.01.012, 2004.

Smith, R. J.: Use and misuse of the reduced major axis for line-fitting, American Journal of Physical Anthropology: The Official Publication of the American Association of Physical Anthropologists, 140, 476–486, https://doi.org/10.1002/ajpa.21090, 2009.

Sprent, P.: Some history of functional and structural relationships, In: BrownPJ, FullerWA, editors. Statistical analysis of measurement error models and applications (contempory mathematics 112). Providence, RI: American Mathematical Society. p 3–15, 1990.

Stober, G., Jacobi, C., Fröhlich, K., and Oberheide, J.: Meteor radar temperatures over Collm (51.3 N, 13 E), Advances in Space Research, 42, 1253–1258, https://doi.org/10.1016/j.asr.2007.10.018, 2008.

475 Thorsen, D., Franke, S. J., and Kudeki, E.: A new approach to MF radar interferometry for estimating mean winds and momentum flux, Radio Science, 32, 707–726, https://doi.org/10.1029/96RS03422, 1997.

Vicente de Julia´n-Ortiz, J., Pogliani, L., and Besalu, E.: Two-variable linear regression: modeling with orthogonal least-squares analysis, Journal of chemical education, 87, 994–995, https://doi.org/10.1021/ed100307z, 2010.

Younger, J. P., Reid, I. M., Vincent, R. A., and Holdsworth, D. A.: Modeling and observing the effect of aerosols on meteor radar measure-
480 ments of the atmosphere, Geophysical research letters, 35, https://doi.org/10.1029/2008GL033763, 2008.

Younger, J. P., Reid, I. M., and Vincent, R. A.: The diffusion of multiple ionic species in meteor trails, Journal of Atmospheric and Solar-Terrestrial Physics, 118, 119–123, https://doi.org/10.1016/j.jastp.2013.10.007, 2014.